U–Pb isotopic ages and Hf isotope composition of zircons in Variscan gabbros from central Spain: evidence of variable crustal contamination

Carlos Villaseca · David Orejana · Elena Belousova · Richard A. Armstrong · Cecilia Pérez-Soba · Teresa E. Jeffries

Abstract Ion microprobe U–Pb analyses of zircons from three gabbroic intrusions from the Spanish Central System (SCS) (Talavera, La Solanilla and Navahermosa) yield Variscan ages (300 to 305 Ma) in agreement with recent studies. Only two zircon crystals from La Solanilla massif gave slightly discordant Paleoproterozoic ages (1,848 and 2,010 Ma). Hf isotope data show a relatively large variation with the juvenile end-members showing εHf_i values as high as +3.6 to +6.9 and +1.5 to +2.9 in the Navahermosa and Talavera gabbros, respectively. These positive εHf_i values up to +6.9 might represent the composition of the subcontinental mantle which generates these SCS gabbros. This εHf_i range is clearly below depleted mantle values suggesting the involvement of enriched mantle components on the origin of these Variscan gabbros, and is consistent with previous whole-rock studies. The presence of zircons with negative εHf_i values suggest variable, but significant, crustal contamination of the gabbros, mainly by mixing with coeval granite magmas. Inherited Paleoproterozoic zircons of La Solanilla gabbros have similar trace element composition (e.g. Th/U ratios), but more evolved Hf-isotope signatures than associated Variscan zircons. Similar inherited ages have been recorded in zircons from coeval Variscan granitoids from the Central Iberian Zone. Granitic rocks have Nd model ages (T_{DM}) predominantly in the range of 1.4 to 1.6 Ga, suggesting a juvenile addition during the Proterozoic. However, Hf crustal model ages of xenocrystic Proterozoic zircons in La Solanilla gabbro indicate the presence of reworked Archean protoliths (T_{DM2} model ages of 3.0 to 3.2 Ga) incorporated into the hybridized mafic magma.

Editorial handling: J. Raith

C. Villaseca (✉) · D. Orejana · C. Pérez-Soba
Departamento de Petrología y Geoquímica-Instituto de Geología Económica. Centro mixto UCM-CSIC,
Complutense University of Madrid,
28040 Madrid, Spain
e-mail: granito@geo.ucm.es

D. Orejana
e-mail: dorejana@geo.ucm.es

C. Pérez-Soba
e-mail: pesoa@geo.ucm.es

E. Belousova
GEMOC, Department of Earth and Planetary Sciences,
Macquarie University,
Sydney, NSW 2109, Australia
e-mail: elena.belousova@mq.edu.au

R. A. Armstrong
Research School of Earth Sciences,
Australian National University,
Canberra, Australia
e-mail: Richard.Armstrong@anu.edu.au

T. E. Jeffries
Department of Mineralogy, Natural History Museum,
London SW7 5BD, UK
e-mail: t.jeffries@nhm.ac.uk

Introduction

Gabbroic intrusions are scarce during the formation of the huge granitic batholiths of late Variscan age which outcrop in western and central Europe (e.g. Liew et al. 1989; Bea et al. 1999). Although minor in volume, their existence reveals mantle participation during this intracontinental orogenic event and is important in the discussion on petrogenetic models of granite generation. In the inner parts of the Iberian Variscan Belt most mafic intrusions have calc-alkaline whole-rock composition. Nevertheless,

the most recent models on their genesis involve a post-collisional within-plate tectonic setting not consistent with subduction during these late stages of the Variscan collision (Scarrow et al. 2009; Órejana et al. 2009).

In central Spain two different models on the origin and nature of the Variscan mafic magmatism have been recently proposed. These magmas have been considered as being formed from primary alkaline mafic melts of appinitic affinity mixed with crustal peraluminous granite magmas during successive emplacement events (Scarrow et al. 2009; Molina et al. 2009). Some mafic-ultramafic facies are rich in exotic accessories, interpreted as crustally-derived xenocrysts (Bea et al. 1999). In a second model, they have been described as calc-alkaline mantle-derived melts reflecting recycling of minor continental crustal components within the mantle, which could exhibit localized crustal contamination (either by assimilation or magma mixing) at the emplacement level (Órejana et al. 2009). Enriched values in the initial Sr-Nd isotopic ratios of the SCS gabbros (e.g. εNd_i ranges from +3.1 to −1.8; Órejana et al. 2009) have been explained by the incorporation of crustal components within the subcontinental mantle lithosphere (1–2% of subducted continental material fits the Sr–Nd isotopic composition of primitive Mg-rich gabbros in central Spain, Órejana et al. 2009). Alternatively, these isotopic ratios could be explained by significant crustal contamination of mantle-derived magmas at the base of the thickened Variscan crust (Bea et al. 1999; Scarrow et al. 2009).

The study of zircon has become a great resource for resolving dating and petrogenetic questions. Zircon is a common accessory mineral in igneous rocks. Its importance lies in a combination of factors: its incorporation of trace elements, its chemical and physical durability and its remarkable resistance to high-temperature diffusive re-equilibration. For these reasons, the precise U–Pb dating, the presence of inheritances, zoning patterns, trace element contents and Hf isotope composition are all used to track magmatic processes (e.g. Belousova et al. 2006; Miller et al. 2007). In this respect, the combined study of mineral chemistry (including Hf isotope composition) and U–Pb geochronology within single zircon grains in gabbroic intrusions is a proven test for evaluating crustal contamination processes (e.g. Peytcheva et al. 2008).

The aim of this work is to better constraint the geochronology of the Variscan gabbros in central Spain and to discuss the role of crustal contamination: during magma transport or by metasomatism in the mantle source. Three gabbro massifs from the Spanish Central System (SCS) were sampled for this study (Talavera, La Solanilla and Navabermosa) (Fig. 1). Mineral chemistry and whole-rock chemical characterization of these mafic massifs, including Sr–Nd–Pb isotopic signatures, have been described previously (Órejana et al. 2009). To our knowledge, this is the first attempt at dating Variscan gabbros in central Spain using SHRIMP methods in combination with LA-ICPMS zircon trace element geochemistry and LA-MC-ICPMS Hf isotope analysis.

Geological setting

The Spanish Central System (SCS) is a mountain range composed mainly of felsic metamorphic rocks and peraluminous granites (e.g. Villaseca et al. 1998; Bea et al. 1999). The SCS peraluminous batholith is one of the major granite outcrops within the Central Iberian Zone, which is the innermost part of the Iberian Variscan Belt (Fig. 1). This felsic batholith mostly comprises monzogranites whose emplacement ages have been estimated in the range of 323 to 284 Ma (whole-rock Rb–Sr, Villaseca et al. 1998 and references therein), post-dating the regional metamorphic peak (around 330 Ma, after Castiñeiras et al. 2008). These intrusions have been classified in three suites: 1) S-type cordierite-bearing granitoids, 2) I-type biotite (amphibole)-bearing granitoids, and 3) transitional biotite granitoids of intermediate peraluminous composition (Villaseca and Herreros 2000). The origin of the SCS granites has been explained as the result of: a) hybridization between crustal melts and mantle-derived magmas (e.g. Pinarelli and Rottura 1995; Moreno-Ventas et al. 1995); b) crustal assimilation of mantle-derived magmas (Ugidos and Recio 1993; Castro et al. 1999); and c) partial melting of mainly crustal sources, either from mid-crustal levels (Bea et al. 1999, 2003) or of lower crustal derivation (Villaseca et al. 1999). A complementary character in composition between SCS granites and some lower crustal granulite xenoliths carried by the SCS Permian alkaline dykes, and the good match in initial Sr–Nd–O–Pb isotope ratios, points to the lower crust as the most likely crustal source for the formation of the SCS batholith (Villaseca et al. 1999, 2007).

The minor mafic intrusions were initially described by Franco and García de Figuerola (1986) and Franco and Sánchez García (1987) in the western SCS and were considered to be the mafic precursors of the felsic granitoids, and the main heat contributors to Variscan metamorphism. Later studies noted the hybridized nature of most of these intrusions due to their coeval intrusion with granitic magmas (e.g. Moreno-Ventas et al. 1995; Montero et al. 2004). In this sense, the gabbroic samples selected for this study are those that are more primitive in composition and apparently uncontaminated (see also Órejana et al. 2009), lacking any petrographical feature of either assimilation with high-grade metamorphic wall-rocks (La Solanilla massif) or hybridization with coeval granite magmas (Talavera and Navahermosa gabbros). Accordingly, there are no felsic cross-cutting dykes or intermediate to felsic enclaves within these primitive gabbroic boulders. In thin section they do not show quartz,

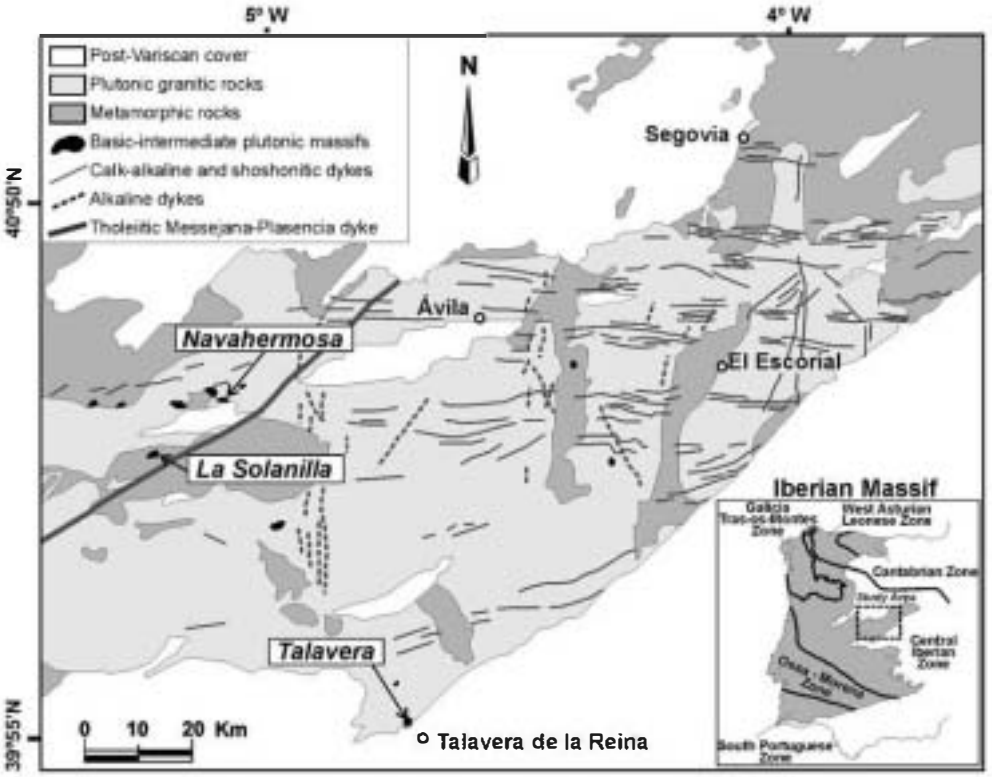

Fig. 1 Geological map of the Spanish Central System showing the location of the studied Variscan gabbros (Talavera, La Solanilla and Navahermosa), modified from Franco and García de Figuerola (1986), Franco and Sánchez García (1987), and Orejana et al. (2009)

K-feldspar or Na-rich plagioclase. Plagioclase is not cellular or spongy in texture and its chemical variation defines a rim to core normal zoning (mostly from An_{68} to An_{36}). Olivine, orthopyroxene and clinopyroxene have high to moderate Mg numbers (0.86 to 0.60), which are close to the composition of later pargasitic amphibole and phlogopitic mica (Orejana et al. 2009).

Initial attempts to date SCS Variscan gabbros by whole-rock Rb-Sr isochrons gave imprecise ages of 416±21 Ma (Pereira et al. 1992), 340±18 Ma (Bea et al. 1999) or 322± 5 Ma (Casillas et al. 1991), reinforcing the "precursor" character assigned to the mafic intrusives. Later works, based on $^{207}Pb/^{206}Pb$ dating of single zircon crystals gave a smaller range of ages; i.e. 319±3 Ma to 310±3 Ma (Bea et al. 2003; Montero et al. 2004). Recent ion microprobe data on mafic intrusions gave a slightly younger age range of 307±2 Ma (Bea et al. 2006) to 305.6±1.4 Ma (Zeck et al. 2007), which clearly overlaps the SCS granite intrusion ages (e.g. Zeck et al. 2007).

Petrographical features

Talavera gabbro

This massif is located in the southernmost part of the SCS (Fig. 1) and was initially described by Martín Parra et al. (1995). It crops out as a 30 m thick, elongated intrusion of medium-to-fine grained massive gabbro in deformed felsic granites; no deformation is observed in the gabbros. Sample T46 is an olivine gabbro with plagioclase, orthopyroxene, clinopyroxene, olivine, pargasitic amphibole and minor phlogopite as major minerals. Common accessories are apatite, titanite, ulvo-spinel, ilmenite, zircon, baddeleyite, baritine and sulphide minerals. Two varieties of baddeleyite and zircon occur in these rocks: either as grains or as lamellar crystals at the rim of large ilmenite crystals, similar to other gabbroic rocks (Naslund 1987; Austrheim et al. 2008; Morisset and Scoates 2008).

Zircon grains appear associated with other accessory phases (e.g. apatite). In zircon separates, the crystals are highly angular, 30 to 250 μm in size (Fig. 2a), representing fragments produced by crushing larger zircons during mineral separation. CL and BSE images reveal bright or light grey domains defining sector or regular oscillatory magmatic zoning. Core sectors have not been found.

La Solanilla gabbro

This gabbro was first described by Franco (1980), and Franco and García de Figuerola (1986) and classified as appinitic gabbro. It was described as mafic precursor of the granitoids. These gabbros, which in the field occur as isolated metre-sized boulders, were intruded into high-grade metamorphic rocks (Fig. 1); they are the only studied mafic intrusions which are not directly related with granites in the field. The sampled gabbro (T115) is a medium grained rock of intergranular texture composed of plagioclase, orthopyrox-

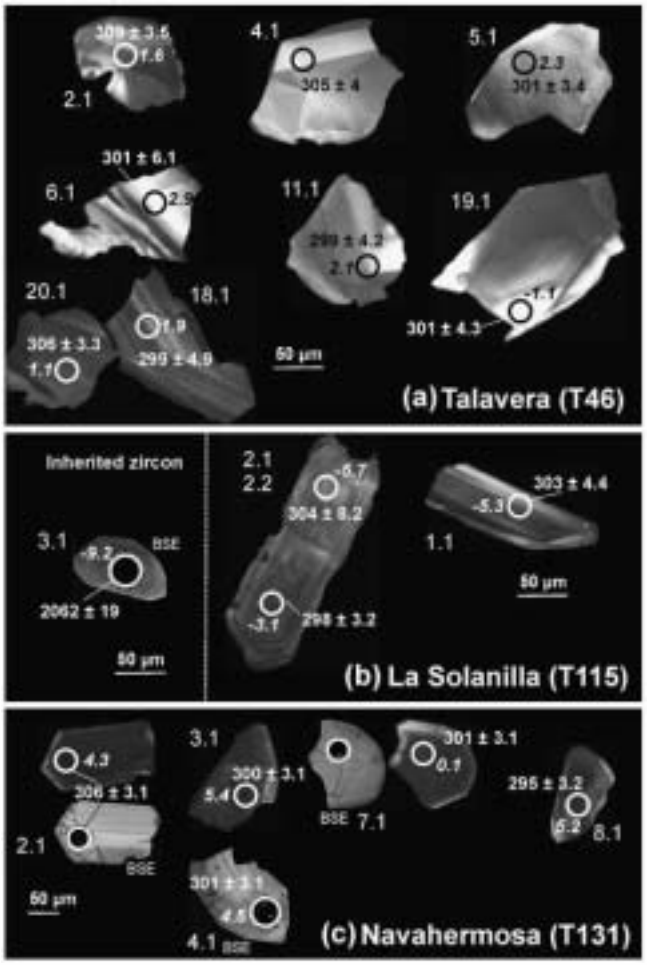

Fig. 2 Cathodoluminiscence (CL) and back-scattered electron (BSE) images of representative zircons from the SCS gabbros. Grain numbers and ages correspond to those listed in Table 1. Analysed εHf_i values (in italics) are also included. **a** Zircon crystals from Talavera sample (T46); some of them showing regular magmatic oscillatory zoning. **b** Zircons from La Solanilla gabbro (T115) can be subdivided into two types: large idiomorphic prisms (with aspect ratios 1:3 to 1:4) (T115, #1–2), and smaller short-prismatic grains (T115, #3BSE), displaying magmatic oscillatory zoning. The short-prismatic crystals give old pre-Variscan ages and are xenocrysts. **c** Zircons from Navahermosa gabbro are angular, ranging in size from 50 to 200 µm (T131). They vary from rounded grains to stubby prisms with magmatic oscillatory zoning

ene, clinopyroxene, olivine, pargasitic amphibole and phlogopite. Olivine is usually surrounded by fined-grained orthopyroxene coronas. Accessory minerals include apatite, ulvo-spinel, ilmenite, zircon, baddeleyite and sulphides. Zircon and baddeleyite occur either as isolated grains or as small lamellar crystals at the rims of large ilmenite crystals.

There are two types of zircon grains in La Solanilla gabbro: a) large (100 250 µm) euhedral elongated prisms (with aspect ratios between 1:3 and 1:4) showing oscillatory magmatic zoning, mainly in the rim (Fig. 2b, T115 # 1 2) and b) small (40 80 µm) stubby dark grains with poorly contrasted zoning (Fig. 2b, T115 # 3). A third variety of zircon occurs as elongated crystals of lamellar aspect defining coronas around ilmenite (Fig. 3). Zircon rims are from a few µm to 10 µm in thickness and are commonly discontinuous along ilmenite grain boundaries (Fig. 3). The magmatic ilmenite is typically surrounded by amphibole or mica, with the thin zircon rim at the very boundary between ilmenite and these hydrous silicates.

Navahermosa gabbro

This massif comprises some small isolated gabbroic outcrops within granodiorite, although most field exposures are restricted to metre-sized, rounded blocks (Fig. 1). It was firstly described and mapped by Franco and Sánchez García (1987) and more recently dated by Zeck et al. (2007) at 305.6± 1.4 Ma. These later authors described the gabbros as massive, medium- to coarse-grained rocks, but in their sampling found that the total modal amount of metamorphic crystals (amphibole, biotite, serpentine, talc, etc) could reach up to 15 vol%, thus classifying the rocks as meta-gabbronorites. The sampled gabbro (T131) contains plagioclase, clinopyroxene, orthopyroxene, olivine, pargasitic amphibole and phlogopite. The original magmatic intergranular texture is well preserved and the low amount of secondary minerals is similar to the other sampled gabbros, which do not show significant metamorphic recrystallization. Accessory minerals are apatite, ilmenite, zircon, baddeleyite and sulphides. Two varieties of zircon were found: a) prismatic grains of 50 to 250 µm; and b) small lamellar crystals (<5 µm) which form discontinuous rims around ilmenite, similar to the other studied gabbros (Fig. 3). More rarely lamellar zircon can also appear as trails inside the ilmenite (Fig. 3). Baddeleyite also appears as lamellar crystals with a similar shape and size as zircon, and occasionally as radiated laths inside ilmenite. Zircon is much more common than baddeleyite in ilmenite rims in all studied gabbros.

Zircon crystals from Navahermosa exhibit a similar angular shape and size range (50 to 200 µm) when compared with those from Talavera (Fig. 2c), although partially displaying euhedral faces. They vary from stubby prisms to rounded grains and display bright thin margins with oscillatory zoning around larger dark areas.

Analytical procedures

Mineral chemistry

Electron microprobe (EMP) analyses were carried out on polished thin sections at the *Centro de Microscopía Electrónica "Luis Bru" (Complutense University of Madrid)*. Before microanalyses, most of the thin sections have been studied using a SEM equipped with an energy-

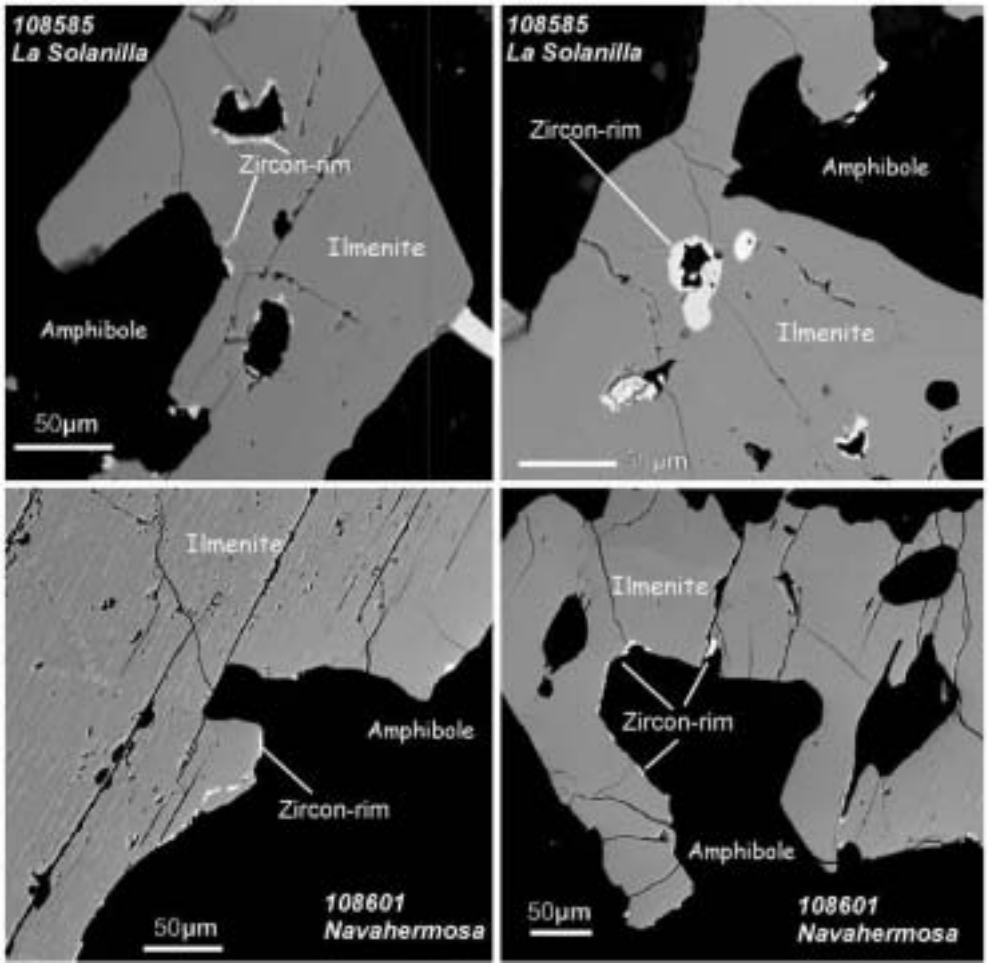

Fig. 3 BSE images of lamellar zircon rims around ilmenite in some Variscan gabbros from the SCS. Most ilmenite is surrounded by late-magmatic H_2O-rich phases, mostly Ti-rich kaersutite (the *black area* of the images, *Amphibole*). Zircon rims do not constitute a continuous thin film around ilmenite, sometimes lamellar zircon appears as trails inside ilmenite

dispersive spectrometric system. Backscattered electron images were used as a guide during microprobe analysis. Zircon major element concentrations were obtained by a wavelength dispersive electron microprobe JEOL Superprobe JXA 8900-M equipped with four crystal spectrometers. Operating conditions were between 15 and 20 kV, a beam current of approximately 50 nA, and spots of 2 µm in diameter. Counting times were set at 20 s on the peak and 10 s on the background for Si and Zr, and 60 s on the peak and 30 s on the background forTi, Al, Fe, Mg, Ca, P, Hf, Th, U and Y. Absolute abundances for each element were determined by comparison with synthetic REE phosphates prepared by Jarosewich and Boatner (1991), and natural minerals for Zr, Y, U and Th. Corrections were made using an on-line ZAF method. Error limits for each element depend strongly on the absolute concentration in each phase but are significant for the <1 wt.% level (with error >10%). Concentrations below 0.2 wt% are merely qualitative. The ThO_2, UO_2, Y_2O_3 and P_2O_5 contents of lamellar zircon around ilmenite (zircon rims) are always below detection limits (0.08 wt% ThO_2, 0.13 wt% UO_2, 0.08 wt% Y_2O_3 and 0.07 wt% P_2O_5).

In situ determinations of concentrations of 30 trace elements (REE, Ba, Rb, Sr, Th, U, Nb, Ta, Pb, Zr, Hf, Y, Sc, V, Co, Zn and Cr) in zircon by laser ablation (LA-ICP-MS) were obtained at the Natural History Museum of London using an Agilent 7500CS ICP-MS coupled to a New Wave UP213 laser source (213 nm frequency-quadrupled Nd-YAG laser). The counting time for one analysis was typically 90 s (40 s measuring gas blank to establish the background and 50 s for the remainder of the analysis). The diameter of the laser beam was around 50 µm. The NIST 612 glass standard was used to calibrate relative element sensitivities for the analyses of the silicate minerals. Each analysis was normalised to Si using concentrations determined by electron microprobe. Detection limits for each element are in the range of 0.01 to 0.06 ppm except for Sc and Cr (0.11 and 0.73 ppm, respectively).

Zircon U Pb dating

Zircons were separated from whole rock using standard crushing and mineral separation techniques, and hand picked before mounting on double-sided tape on glass slides in 1×6 mm parallel rows together with some chips of zircon standard TEMORA 1 (Black et al. 2003). After

setting in epoxy resin, zircons were ground down to expose their central portions and imaged with transmitted and reflected light on a petrographic microscope, and with cathodoluminescence on a HITACHI S2250-N scanning electron microscope (housed at ANU-Canberra) to identify internal structure, inclusions, fractures and physical defects. Lamellar zircon, due to its extremely small size (<10 μm), was not possible to concentrate.

Zircon U–Pb analyses were done using a Sensitive High Resolution Ion Microprobe-Reverse Geometry (SHRIMP-RG) at the Research School of Earth Sciences, Australian National University, following procedures given in Williams (1998, and references therein). Each analysis consisted of six scans through the relevant mass range with the TEMORA reference zircon grains analysed for every three unknown analyses. Secondary ions are generated from the target spot with an O^{2-} primary ion beam which typically produces a spot with a diameter of ~20 μm and a depth of 0.5–1 μm.

Data were reduced using the SQUID Excel Macro of Ludwig (2001). The Pb/U ratios were normalised to a value of 0.0668 for the TEMORA reference zircon, equivalent to an age of 417 Ma (Black et al. 2003). Concentration data are normalized against zircon standard SL13 (210 ppm U, Black et al. 2004). Uncertainties given in Table 1 for individual analyses are at the 1σ level. Wetherill (1956) and Tera and Wasserburg (1972) Concordia plots and weighted mean calculations were carried out using Isoplot 3.0 software (Ludwig 2003), with uncertainties reported as 95% confidence limits.

Zircon Lu–Hf isotope analysis

Hf isotope analyses were carried out in situ using a New Wave Research LUV213 laser-ablation microprobe, attached to a Nu Plasma multi-collector ICPMS at GEMOC, Macquarie University, Sydney. The laser system delivers a beam of 213 nmUV light from a frequency-quintupled Nd:YAG laser. Analyses were carried out with a beam diameter of 40 to 55 μm, a 5 Hz repetition rate, and energies of about 0.1 mJ. This results in total Hf signals of ~$1–6\times10^{-11}$A, depending on conditions and Hf contents. Typical ablation times are 100–120 s, resulting in pits 30–40 μm deep. He carrier gas transports the ablated sample from the laser-ablation cell via a mixing chamber (Ar) to the ICPMS torch. The Nu Plasma MC-ICPMS features and other analytical techniques are those described by Griffin et al. (2002, 2004). The same spots analysed by SHRIMP were targeted for Hf analysis.

To evaluate the accuracy and precision of the laser-ablation results, and to test the reliability of the correction protocols, we have repeatedly analysed two zircon standards, 91500 and Mud Tank (MT). These reference zircons gave $^{176}Hf/^{177}Hf$= 0.282317±0.000041 (2σ) and 0.282505±0.000044 (2σ), respectively, which are identical to average published values on solutions (0.282306±0.000008 for 91500 and 0.282507± 0.000006 for MT, Woodhead and Hergt 2005). The 2σ uncertainty on a single analysis of $^{176}Lu/^{177}Hf$ is ±0.001–0.002% (about 1 epsilon unit), reflecting both analytical uncertainties and the spatial variation of Lu/Hf across many zircons. The ^{176}Lu decay constant value of $1.865\times10^{-11}a^{-1}$ was used in all calculations (Scherer et al. 2001). Chondritic $^{176}Hf/^{177}Hf$=0.282772 and $^{176}Lu/^{177}Hf$=0.0332 (Bouvier et al. 2008) and the depleted mantle $^{176}Hf/^{177}Hf$ = 0.28325 (ε_{Hf}=+16.4) and $^{176}Lu/^{177}Hf$=0.0384 were applied to calculate ε_{Hf} values and model ages used in this work.

Results

U–Pb zircon ages

The whole analytical data set is listed in Table 1 and plotted in Tera-Wasserburg Concordia diagrams (Fig. 4). Ages younger than 1,000 Ma are 204-corrected $^{206}Pb/^{238}U$, whereas older ages are 204-corrected $^{207}Pb/^{206}Pb$ (only two analyses in this case, Table 1).

Twenty U–Pb analyses were performed on different zircon grains from Talavera sample T46 (Table 1). On a Tera-Wasserburg diagram they plot concordantly and the weighted mean of the radiogenic $^{206}Pb/^{238}U$ ages is 305.4± 3.2 Ma with no excess scatter (MSWD=0.94) (Fig. 4). This age is interpreted as the emplacement age of the Talavera gabbro.

Only four zircon grains have been separated from La Solanilla (sample T115). Five U–Pb analyses were performed on these four zircon grains. Three data from elongated prisms are concordant whereas the two small stubby grains give discordant ages of 1,848±5 and 2,010± 12 Ma, although they show less than 10% discordancy. Weighted mean of the three concordant data yields an age of 300.3±5.5 Ma (MSWD=0.62) (Fig. 4). However, zircon grains from this sample are crustal-derived antecrysts, as will be discussed below. Thus, the above data must represent a maximum value for the gabbro emplacement age.

Eight analyses were obtained on eight different zircon grains from Navahermosa (sample T131). The mean $^{206}Pb/^{238}U$ age is 301±3.4 Ma with no excess scatter (MSWD=1.4) (Fig. 4). This age is within error of that obtained by Zeck et al. (2007) for the same gabbro massif (305.6±1.4 Ma).

Zircon trace element composition

Zircons with high Th/U values are recorded both by laser analyses and SHRIMP data. However, Th/U ratios deter-

Table 1 U–Th–Pb SHRIMP data of zircon, SCS Variscan gabbros

Spot number	Common ^{206}Pb (%)	U (ppm)	Th (ppm)	Th/U	$^{238}U/^{206}Pb$	±%	$^{207}Pb/^{206}Pb$	±%	$^{238}U/^{206}Pb^{a}$	±%	$^{207}Pb/^{206}Pb^{a}$	±%	$^{206}Pb/^{238}U$	±%	$^{206}Pb/^{238}U$ age		$^{207}Pb/^{206}Pb$ age	
Talavera (T46)																		
1.1	0.216	59	0.34	0.01	20.82613	1.7	0.05411	3.5	20.82613	1.7	0.05411	3.5	0.04802	1.7	302	±5.1	376	± 78
2.1	<0.001	324	192	0.61	20.33039	1.2	0.05194	1.5	20.36907	1.2	0.05041	2.3	0.04909	1.2	309	±3.5	214	± 54
3.1	0.370	111	73	0.68	20.36931	1.4	0.05549	2.6	20.36931	1.4	0.05549	2.6	0.04909	1.4	309	±4.4	432	± 57
4.1	0.403	150	103	0.71	20.52033	1.3	0.05570	2.2	20.62622	1.3	0.05157	3.2	0.04848	1.3	305	±4	266	± 74
5.1	<0.001	339	189	0.58	20.91088	1.2	0.05215	1.5	20.91088	1.2	0.05215	1.5	0.04782	1.2	301	±3.4	292	± 34
6.1	0.474	108	103	0.99	20.91335	2.1	0.05613	2.9	20.91335	2.1	0.05613	2.9	0.04782	2.1	301	±6.1	458	± 64
7.1	<0.001	95	76	0.83	20.58697	1.5	0.05214	2.8	20.58697	1.5	0.05214	2.8	0.04857	1.5	306	±4.5	291	± 64
8.1	<0.001	98	82	0.87	20.77927	1.5	0.04981	2.8	20.77927	1.5	0.04981	2.8	0.04812	1.5	303	±4.4	186	± 66
9.1	<0.001	102	75	0.76	20.48097	1.6	0.05246	2.7	20.48097	1.6	0.05246	2.7	0.04883	1.6	307	±4.7	306	± 61
10.1	0.121	154	113	0.76	20.70207	1.4	0.05339	2.2	20.77036	1.4	0.05074	4.1	0.04815	1.4	303	±4.2	229	± 94
11.1	0.129	140	140	1.03	21.09175	1.4	0.05333	4.3	21.09175	1.4	0.05333	4.3	0.04741	1.4	299	±4.2	343	± 97
12.1	0.823	168	217	1.34	20.40556	1.3	0.05908	2	20.57166	1.4	0.05259	6.4	0.04861	1.4	306	±4.1	311	±140
13.1	0.195	285	199	0.72	20.57451	1.2	0.05403	1.6	20.59415	1.2	0.05326	1.8	0.04856	1.2	306	±3.6	340	± 40
14.1	0.038	274	299	1.13	20.16064	1.2	0.05291	1.7	20.19053	1.2	0.05172	1.9	0.04953	1.2	312	±3.7	273	± 43
15.1	0.106	181	192	1.10	20.36451	1.3	0.05338	2.1	20.36451	1.3	0.05338	2.1	0.04911	1.3	309	±3.9	345	± 47
16.1	0.518	129	123	0.98	20.39889	1.4	0.05665	2.3	20.55772	1.4	0.05043	6.2	0.04864	1.4	306	±4.3	215	±140
17.1	<0.001	139	111	0.82	20.53080	1.4	0.05202	2.4	20.53080	1.4	0.05202	2.4	0.04871	1.4	307	±4.1	286	± 55
18.1	0.288	478	565	1.22	21.02436	1.7	0.05461	1.3	21.05614	1.7	0.05340	1.8	0.04749	1.7	299	±4.9	346	± 41
19.1	0.497	115	98	0.89	20.80874	1.4	0.05635	2.5	20.89192	1.5	0.05316	4.5	0.04787	1.5	301	±4.3	336	±100
20.1	0.037	663	906	1.41	20.58892	1.1	0.05276	1.1	20.58892	1.1	0.05276	1.1	0.04857	1.1	306	±3.3	318	± 25
La Solanilla (T115)																		
1.1	0.03	524	320	0.63	20.77366	1.5	0.05262	1.2	20.77366	1.5	0.05262	1.2	0.04814	1.5	303	± 4.4	313	±27
2.1	<0.001	336	94	0.29	20.69336	2.8	0.05154	1.5	20.69336	2.8	0.05154	1.5	0.0483	2.8	304	± 8.2	265	±35
2.2	<0.001	567	158	0.29	21.14600	1.1	0.05205	1.2	21.13086	1.1	0.05263	1.3	0.04732	1.1	298	± 3.2	313	±30
3.1	<0.001	355	72	0.21	2.65297	1.1	0.12383	0.68	2.65342	1.1	0.12368	0.69	0.37687	1.1	2,062	±19	2,010	±12
4.1	1.03	1,268	789	0.64	3.26041	1.0	0.11361	0.28	3.26272	1.0	0.11300	0.3	0.30649	1.0	1,723	±16	1,848	± 5
Navahermosa (T131)																		
1.1	0.32	1,010	635	0.65	21.12118	1.5	0.05482	1.1	21.14814	1.5	0.05380	1.3	0.04729	1.5	298	±4.5	363	±30
2.1	0.13	2,695	1,839	0.71	20.51994	1.0	0.05352	0.46	20.55029	1.0	0.05234	0.66	0.04866	1.0	306	±3.1	300	±15
3.1	0.04	956	848	0.92	21.00363	1.1	0.05268	0.92	21.02381	1.1	0.05191	0.99	0.04757	1.1	300	±3.1	281	±23
4.1	0.02	1,332	861	0.67	20.89399	1.0	0.05249	1.3	20.89399	1.0	0.05249	1.3	0.04786	1.0	301	±3.1	307	±29
5.1	0.02	807	359	0.46	20.61572	1.1	0.0526	0.94	20.61330	1.1	0.05269	0.95	0.04851	1.1	305	±3.2	316	±22
6.1	<0.001	2,177	3,922	1.86	21.19644	1.0	0.05218	0.6	21.20064	1.0	0.05203	0.61	0.04717	1.0	297	±3	287	±14
7.1	0.05	1,154	551	0.49	20.89012	1.1	0.05277	0.82	20.89012	1.1	0.05277	0.82	0.04787	1.1	301	±3.1	319	±19
8.1	0.43	528	227	0.44	21.27781	1.1	0.05564	1.1	21.35893	1.1	0.05259	1.7	0.04682	1.1	295	±3.2	311	±39

All errors are 1σ

[a] Radiogenic lead ^{204}Pb corrected for common lead

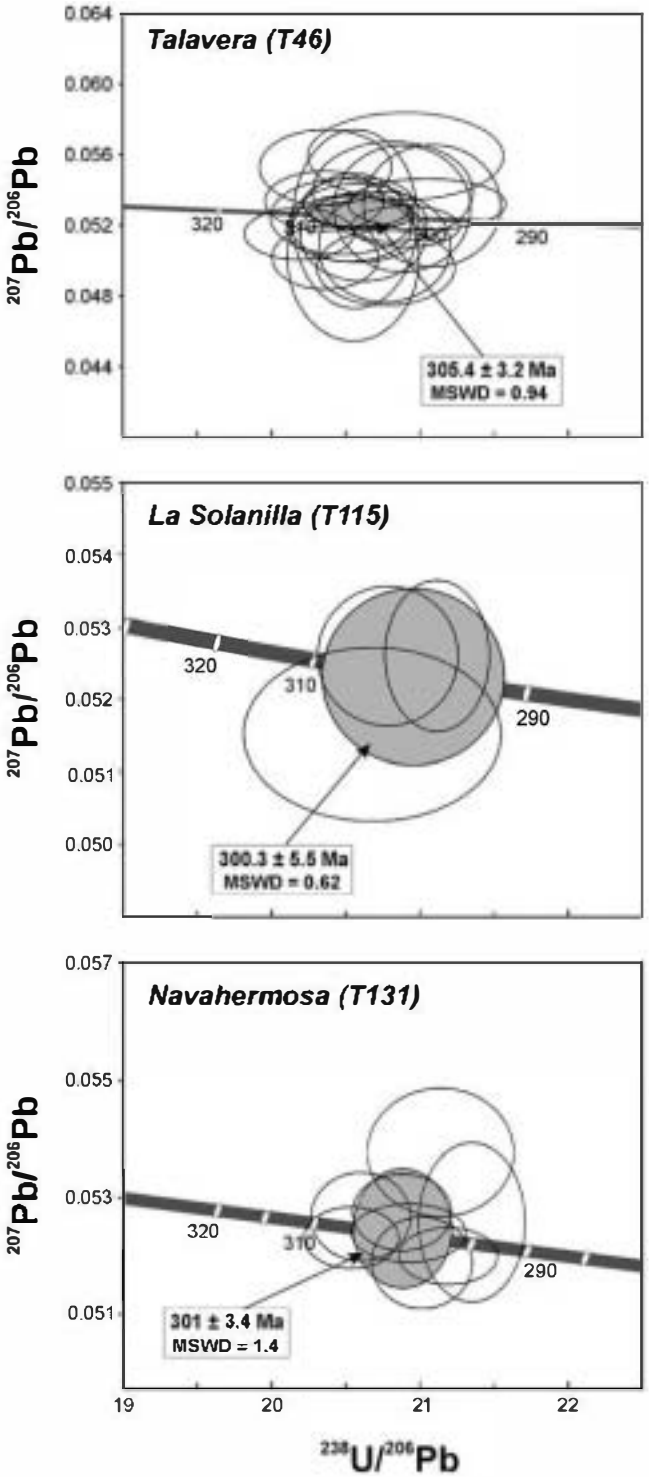

Fig. 4 Tera-Wasseburg diagrams with data for the SCS Variscan gabbros. Grey ellipses correspond to the weighted mean ages (error ellipses are ± 2σ)

mined by LA-ICPMS methods are slightly higher to those obtained by SHRIMP-RG techniques (Tables 1 and 2), as absolute values between both methods could differ by to up to three times. Th and U contents discussed throughout the text refer to data obtained by LA-ICPMS.

Zircons from the three samples show some distinctive chemical features. Zircon from Navahermosa gabbro have higher Th, U and Pb contents than those from the other massifs (Fig. 5) (Table 2), in agreement with the corresponding higher Th, U and Pb whole-rock contents of these rocks (Orejana et al. 2009). Zircon from La Solanilla gabbro shows the highest Hf, Ga, Ta, Nb and Sc contents (Table 2). The chondrite-normalised REE pattern of zircon from the studied gabbros (Fig. 6) shows a similar trend with a marked enrichment of HREE over MREE (Gd_N/Yb_N= 0.18 0.02 for Yb_N= 116 6966) and LREE. A positive Ce anomaly (Ce/Ce*= 1.75 111.8) is observed and also a negative Eu anomaly of variable magnitude (Eu/Eu*= 0.02 0.38), except for three grains from the Navahermosa gabbro, which has no Eu anomaly or a positive one (grains 3.1 and 6.1, Table 2, with Eu/Eu*= 1.3 to 2.0). The lack of negative Eu anomaly suggests zircon crystallization in the absence of plagioclase (see Renna and Tribuzio 2009).

The stubby grains of La Solanilla gabbro are much older than the Variscan magmatic zircon and they are presumably xenocrystic. These inherited zircons from La Solanilla have similar composition when compared with the large idiomorphic zircon grains from the same sample (Fig. 5), although slightly lower U, Th, Y and HREE concentrations are detected (Table 2). Nevertheless, their Th/U ratios clearly overlap those of the elongated zircons (0.24 0.70 and 0.35 0.65, respectively). These high Th U ratios in zircons from La Solanilla are suggestive of magmatic crystallization (Hoskin and Schaltegger 2003). One of the inherited zircons from La Solanilla (T115-3.1) has a marked flat HREE pattern (Fig. 6), suggestive of equilibration with another HREE-bearing phase (garnet, xenotime) (e.g. Rubatto and Hermann 2007).

Ti-in-zircon temperature estimates

The direct application of Ti concentration to calculation of zircon crystallization temperatures of mafic rocks is still a matter of debate because it usually gives too low temperature estimates (Watson et al. 2006; Fu et al. 2008). Corrected Ti-in-zircon crystallization temperatures using the recalibrated Ti-in-zircon equation of Ferry and Watson (2007) have been calculated for the analyzed zircons (Table 2). Based on the general absence of rutile and quartz in these gabbros, implying that both a_{TiO_2} and a_{SiO_2} are <1, we have assumed intermediate a_{TiO_2} and a_{SiO_2} values of 0.7 for all samples, comparable to those used in other quartz-undersaturated gabbros lacking feldspathoids (e.g. Watson et al. 2006; Grimes et al. 2009). Calculated values result in a moderate increase in calculated temperatures of a maximum of 10°C as compared to those assuming a_{TiO_2} and a_{SiO_2}=1, because reduced activities of SiO_2 and TiO_2 compensate for one another in terms of their effect in calculated *T* (Ferry and Watson 2007). The pressure dependence of the Ti-in-zircon

Table 2 Representative zircon trace element (LA-ICPMS) composition (in ppm), SCS Variscan gabbros

Massif	Talavera (T46)				Solanilla (T115)					Navahermosa (T131)				
Sample	4.1	7.1	14.1	20.1	2.1	1.1	2.2	3.1 inher.	4.1 inher.	1.1	3.1	4.1	6.1	7.1
Sc	186	173	193	185	299	368	292	417	164	175	176	295	210	180
Cr	1.95	2.64	2.15	2.39	2.33	2.60	1.71	2.19	1.81	2.83	1.99	2.05	2.25	1.74
Ti	7.79	11.21	22.18	11.69	3.96	7.01	6.41	10.61	13.97	3.30	3.18	4.14	4.38	2.28
Rb	0.15	0.08	0.23	0.21	0.16	0.51	0.09	0.10	0.06	0.11	0.17	0.23	0.27	0.11
Sr	0.10	0.10	0.19	0.20	0.23	0.30	0.18	0.11	0.15	0.18	0.34	0.17	0.25	0.13
Ba	0.06	0.08	0.02	0.07	0.03	0.57	0.11	0.09	0.09	0.11	0.22	0.09	0.13	0.18
Nb	0.29	0.49	1.82	0.74	4.68	3.42	3.53	0.51	7.34	0.19	0.11	4.71	0.51	0.22
Ta	0.26	0.44	1.20	0.78	4.52	2.48	3.05	0.28	2.93	0.13	0.11	8.79	1.11	0.45
Hf	12,700	13,800	11,100	12,200	19,100	19,100	19,500	19,600	18,300	7,740	10,800	9,940	11,400	9,950
Pb	4.37	2.71	12.80	14.2	3.02	7.64	3.32	5.44	27.2	34.5	23.6	39.0	98.6	32.7
Th	261	146	663	865	181	444	225	47.3	239	1,950	1,300	2,160	5,540	1,790
U	138	93.4	274	403	524	680	457	201	340	1,540	882	1,690	2,020	1,280
Y	1,050	1,180	3,090	2,540	2,090	4,350	1,610	1,110	603	1,400	943	2,780	3,870	2,050
La	0.012	0.026	0.137	0.10	0.039	0.261	0.071	0.023	0.034	0.208	0.791	0.071	0.566	0.020
Ce	4.42	6.49	12.4	10.2	6.32	8.75	8.76	0.954	37.5	7.23	7.08	54.5	18	8.68
Pr	0.121	0.198	0.593	0.746	0.021	0.529	0.077	0.102	0.091	0.347	0.553	0.357	0.654	0.089
Nd	1.80	3.93	9.1	10.2	0.97	8.25	0.811	2.35	1.17	3.27	4.52	6.08	8.55	2.01
Sm	4.25	6.24	15.6	14.2	3.23	15.4	3.06	7.97	1.62	3.68	3.91	12.9	13.7	4.57
Eu	0.698	0.811	2.06	1.94	0.19	1.32	0.2	0.2	0.3	1.52	4.53	3.53	4.94	1.0
Gd	21.8	29.6	73.5	64.2	27.8	102	23.4	55	8.19	23.4	19.5	99.8	90.8	31
Tb	7.01	8.9	23.7	19.8	11	32.4	9.38	16.3	2.88	7.5	6.17	30.6	29.3	11.4
Dy	89.2	110	285	233	163	418	131	146	42.6	102	75	322	352	155
Ho	31.8	37.6	99	78.2	67.3	150	52.7	34.5	18.2	39.7	27.8	91.2	118	60.3
Er	148	168	441	346	334	670	254	104	94.9	193	135	315	483	278
Tm	31	33.6	89.4	69.9	75.6	136	57.2	16.2	23.8	43.2	30.7	56.2	95.2	59
Yb	287	289	756	608	689	1,150	530	114	230	400	302	442	779	501
Lu	58.4	52.8	141	111	141	219	105	18.9	47.4	81.6	61.8	69.9	134	94.1
T_1 (°C)	719	751	816	755	666	711	703	746	771	652	649	669	673	626
T_2 (°C)	774	810	885	814	713	764	756	804	833	698	695	717	723	669

inher. = inherited (Proterozoic) zircon. T_1 after Watson et al. (2006). T_2 after Ferry and Watson (2007) using $aSiO_2$=0.7, $aTiO_2$=0.5 and P=0.3 Kb

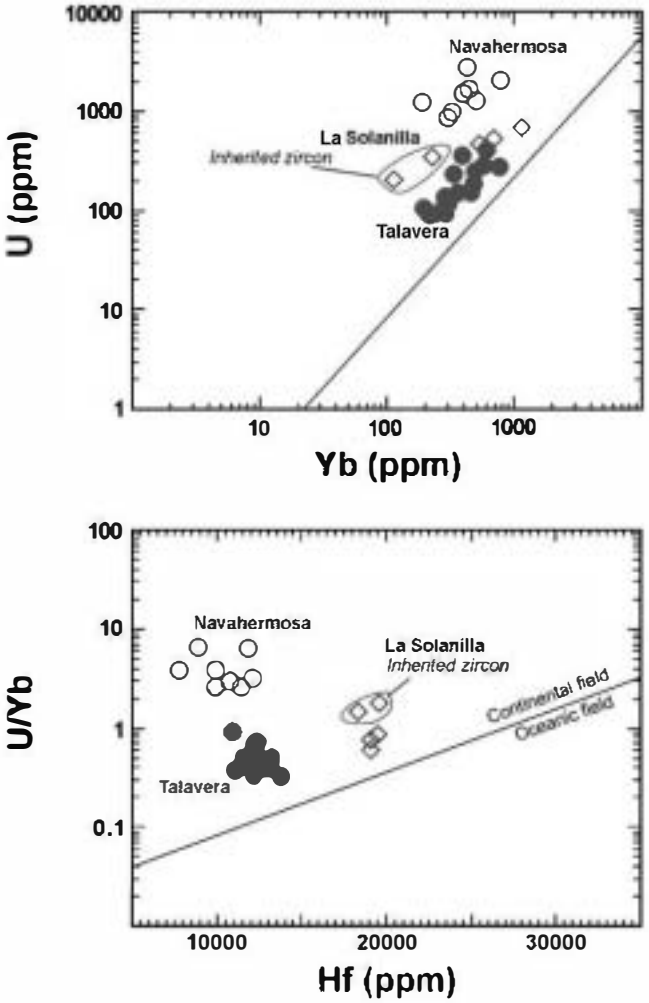

Fig. 5 Zircon trace element composition (LA-ICPMS) from the SCS Variscan gabbros. All zircons plot in the continental field of Grimes et al. (2007) and define distinct fields for each gabbro massif. Inherited zircon from La Solanilla is similar in composition to associated magmatic crystals (see also in the text)

temperature is below 50°C/GPa (Ferry and Watson 2007). Geobarometric estimates for the crystallization of the SCS gabbros (0.3–0.4 GPa; Molina et al. 2009), would result in a T increase of 20°C. Using these maximum temperature estimates (Table 2), only zircons from Talavera gabbros would give a T range (from 770°C to 885°C) which overlaps temperatures estimated by amphibole-plagioclase thermometry in the SCS gabbros (825°C to 970°C; Molina et al. 2009). The other two gabbros give temperatures mostly below solidus conditions of mafic magmas (665°C to 830°C) (Table 2). This is in agreement with the general statement that Ti-in-zircon temperatures on gabbros usually underestimate the true crystallization conditions due to some combination of calibration uncertainties and factors that have not been accurately corrected for (e.g. Fu et al. 2008; Grimes et al. 2009). Alternatively, a xenolithic origin of zircons from La Solanilla gabbro and for some zircon crystals from Navahermosa gabbro (see discussion below) could explain their low T estimates, which are in the range of geothermometric estimates in coeval monzogranitic to granodioritic magmas (662°C to 690°C; Scarrow et al. 2009).

Lamellar Zr-rich minerals

The presence of Zr-rich minerals forming rims around ilmenite is suggestive of the Zr-rich character of the

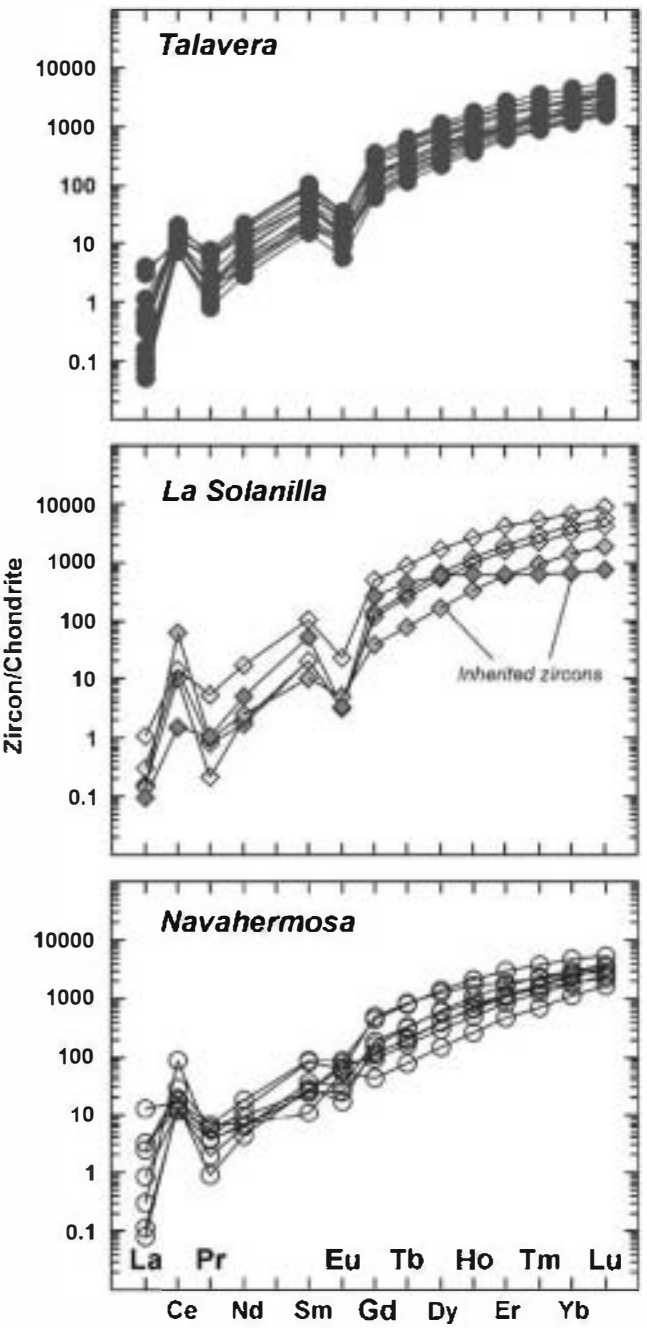

Fig. 6 REE chondrite normalized plots of zircons from the SCS Variscan gabbros. Data were normalized using C1 values of Sun and McDonough (1989)

magmatic ilmenite, as occurs in other mafic intrusions (e.g. Naslund 1987; Morisset and Scoates 2008).

Some trace elements analyzed in situ by EMP in lamellar zircon are always below detection limits (0.08 wt% ThO_2; 0.13 wt% UO_2; 0.08 wt% Y_2O_3) (Table 3). Consequently, zircon around ilmenite shows significantly lower Th, U and Y contents than magmatic zircon grains (Table 3). On the contrary, they have higher Ti and Fe contents than isolated zircon grains, although displaying large variations. Baddeleyite in ilmenite rims also shows significant FeO and TiO_2 contents (up to 1.4 and 1.1 wt%, respectively) when compared with isolated baddeleyite grains. These high Ti–Fe contents may result from the effects of secondary fluorescence in those extremely small lamellar zircon (mostly <5 μm), which are interstitial to Ti–Fe-rich minerals (ilmenite, mica, amphibole) (Morisset and Scoates 2008).

The lack of textural relationships between baddeleyite and zircon in the observed ilmenite rims suggests that zircon formation by exsolution of baddeleyite from Fe–Ti oxide and subsequent reaction is unlikely in the studied gabbros. Moreover, the extremely low Hf, Th and U contents of zircon rims indicate that evolved magmatic liquids are not involved in its genesis. Zircon rims are clearly related to a complex corona replacement around ilmenite which also involves amphibole or phlogopite but is neither associated to low-temperature secondary minerals or to late infiltrating hydrothermal fluids (Fig. 3). The diffusion of Zr in ilmenite would be enhanced by the high temperature during early subsolidus conditions. Silica to form zircon was provided by adjacent silicate minerals. As predicted by recent studies, zircon around ilmenite is a common feature in slowly cooled mafic plutonic rocks (Morisset and Scoates 2008).

Hf isotope composition

The whole analytical data set is listed in Table 4. The εHf values are calculated for the corresponding age, as determined by the U–Pb method.

Zircons from the Talavera gabbros show a wide range of $^{176}Lu/^{177}Hf$ ratios, although all values are below 0.0035, and $^{176}Yb/^{177}Hf$ <0.15 for all analyses (Table 4). They give a narrow range of initial $^{176}Hf/^{177}Hf$ from 0.282551 to 0.282665 (Fig. 7). This corresponds to initial εHf values ranging from −1.1 to +2.9, with most values close to +2± 0.9, within the precision of the laser ablation method (Table 4). Nevertheless, the total variation in the epsilon values points to multiple magma sources in zircon formation. The Nd isotope composition, with initial whole-rock εNd of −1.6 (Orejana et al. 2009), is clearly lower than Hf results. The Hf model ages (T_{DM}) calculated using the zircon Lu/Hf ratios (0.82 to 1.02 Ga) are also below values calculated with the whole-rock Nd model age (1.27 to 1.45 Ga) (Orejana et al. 2009).

Navahermosa zircons show considerable compositional variation that is not supported by the observed narrow Lu/Hf ratios, and might be due to differences in initial

Table 3 Representative zircon major element (EMP) composition (in wt%), SCS Variscan gabbros

Sample	Talavera			La Solanilla				Navahermosa		
	107038-9 rim	107038-10 rim	107038-11 grain	108585-3 rim	108585-5 rim	108585-4 rim	108585 grain	108601-1 rim	108601-3 rim	108601 grain
SiO_2	32.80	32.38	32.34	31.14	31.91	31.57	32.03	32.10	32.49	31.85
TiO_2	0.13	0.19	bdl	0.85	0.75	0.49	bdl	1.14	0.37	bdl
Al_2O_3	bdl	bdl	bdl	bdl	bdl	bdl	bdl	bdl	0.19	bdl
FeO	0.51	0.40	bdl	1.13	1.09	1.02	bdl	1.29	1.19	bdl
MgO	bdl	bdl	bdl	bdl	bdl	bdl	bdl	bdl	0.27	bdl
CaO	bdl	bdl	bdl	bdl	bdl	bdl	bdl	bdl	0.39	bdl
ZrO_2	65.61	66.23	66.87	66.22	66.17	65.02	66.34	64.32	63.68	64.75
HfO_2	1.31	0.20	1.04	0.88	0.89	0.90	1.43	0.93	1.11	1.05
ThO_2	bdl	bdl	0.03[a]	bdl	bdl	bdl	0.04[a]	bdl	bdl	0.43
UO_2	bdl	bdl	0.03[a]	bdl	bdl	bdl	0.06[a]	bdl	bdl	0.23
Y_2O_3	bdl	bdl	0.08[a]	bdl	bdl	bdl	0.35	bdl	bdl	0.33
P_2O_5	bdl	bdl	0.08	bdl	bdl	bdl	0.07	bdl	bdl	0.14
Total	100.19	99.34	100.38	100.30	100.81	99.00	100.32	99.76	99.68	98.82

Zircon types are those in ilmenite rims (rims) or in isolated grains (grains)

bdl below detection limits

[a] Data from LA-ICPMS (they are below EMP detection limits)

Table 4 Lu-Hf isotope data on zircons, SCS Variscan gabbros

Sample	$^{176}Hf/^{177}Hf$	2SE	$^{176}Lu/^{177}Hf$	2SE	$^{176}Yb/^{177}Hf$	Age (Ma)	$(^{176}Hf/^{177}Hf)_i$	εHf_i	2SE	T_{DM}	T_{DM2}[a]
Talavera											
T46-11.1	0.282652	0.000036	0.0018	0.00006	0.085	305	0.282642	2.1	1.2	0.87	1.19
T46-18.1	0.282641	0.000018	0.0008	0.00004	0.036	305	0.282636	1.9	0.6	0.86	1.20
T46-19.1	0.282568	0.000048	0.0031	0.00011	0.149	305	0.282551	−1.1	1.7	1.02	1.40
T46-2.1	0.282638	0.000026	0.0016	0.00001	0.070	305	0.282629	1.6	0.9	0.88	1.22
T46-20.1	0.282617	0.000036	0.0008	0.00007	0.036	305	0.282613	1.1	1.2	0.89	1.26
T46-3.1	0.282665	0.000030	0.0009	0.00004	0.041	305	0.282660	2.7	1.0	0.83	1.15
T46-5.1	0.282655	0.000048	0.0011	0.00001	0.044	305	0.282649	2.3	1.7	0.85	1.18
T46-6.1	0.282667	0.000036	0.0004	0.00001	0.016	305	0.282665	2.9	1.3	0.82	1.14
T46-7.1	0.282645	0.000030	0.0012	0.00001	0.062	305	0.282638	2.0	1.1	0.87	1.20
T46-8.1	0.282636	0.000028	0.0021	0.00009	0.104	305	0.282624	1.5	1.0	0.90	1.23
La Solanilla											
T115-1.1	0.282444	0.000028	0.0016	0.00009	0.063	300	0.282435	−5.3	1.0	1.16	1.66
T115-1.1.2	0.282464	0.000030	0.0016	0.00006	0.068	300	0.282455	−4.6	1.1	1.13	1.61
T115-2.1	0.282433	0.000034	0.0014	0.00015	0.046	300	0.282425	−5.7	1.2	1.17	1.68
T115-2.2	0.282503	0.000028	0.0010	0.00005	0.045	300	0.282497	−3.1	1.0	1.06	1.52
T115-3.1	0.281248	0.000028	0.0001	0.00001	0.006	2,010	0.281244	−9.2	1.0	2.73	3.23
T115-4.1	0.281479	0.000076	0.0025	0.00015	0.090	1,848	0.281390	−7.7	2.7	2.58	3.01
Navahermosa											
T131-1.1	0.282785	0.000054	0.0010	0.00003	0.055	301	0.282779	6.9	1.9	0.66	0.88
T131-2.1	0.282711	0.000050	0.0008	0.00007	0.038	301	0.282707	4.3	1.8	0.76	1.05
T131-3.1	0.282746	0.000040	0.0014	0.00002	0.055	301	0.282738	5.4	1.4	0.72	0.98
T131-3.1.2	0.282714	0.000042	0.0010	0.00003	0.041	301	0.282709	4.4	1.5	0.76	1.04
T131-4.1	0.282685	0.000048	0.0014	0.00012	0.068	301	0.282677	3.3	1.7	0.81	1.11
T131-5.1	0.282629	0.000036	0.0010	0.00002	0.057	301	0.282623	1.3	1.2	0.88	1.24
T131-6.1	0.282697	0.000036	0.0016	0.00010	0.058	301	0.282688	3.6	1.2	0.80	1.09
T131-7.1	0.282595	0.000032	0.0014	0.00005	0.062	301	0.282587	0.1	1.1	0.94	1.32
T131-8.1	0.282738	0.000054	0.0008	0.00005	0.036	301	0.282733	5.2	1.9	0.73	0.99

[a] T_{DM2} is two-stage Hf model ages calculated using an averaged crustal Lu/Hf ratio of 0.015 (Griffin et al. 2002)

$^{176}Hf/^{177}Hf$. The range in $(^{176}Hf/^{177}Hf)_i$ is 0.282587 to 0.282779 (Fig. 7), which corresponds to initial ε_{Hf} values ranging from +0.1 to +6.9, a total variation of 7 epsilon units (Fig. 8). The initial whole-rock εNd of +1.3 to +1.8 is within the range of Hf data. The Hf model ages (0.66 to 0.94 Ga) are similar to whole-rock Nd model ages (0.99 to 1.08 Ga) from Navahermosa gabbros (Orejana et al. 2009).

The data reveal a distinctly unradiogenic overall zircon Hf isotope composition in the La Solanilla gabbro. The Variscan zircons have a range of $(^{176}Hf/^{177}Hf)_i$ from 0.282425 to 0.282497, which corresponds with initial εHf values ranging from −3.1 to −5.7. Proterozoic inherited zircons show a more evolved Hf isotope composition with $^{176}Hf/^{177}Hf_i$ from 0.281244 to 0.281390, and a range of −7.7 to −9.2 in initial ε_{Hf} values (Table 4; Figs. 7 and 8). In clear disagreement with Hf results, the whole-rock Nd isotope data gave the most radiogenic values found in any Variscan gabbro from the Central Iberian Zone: εNd_i=+2.4 to +3.1 (Orejana et al. 2009).

Discussion

Geochronology of mafic magmatism

Most of the analyzed zircons cluster in a narrow range of Variscan ages (300 to 305 Ma) in agreement with previous geochronological studies (Bea et al. 2006; Zeck et al. 2007). Intrusion ages coincide with previous U–Pb SHRIMP zircon data on Navahermosa gabbros published by Zeck et al. (2007). Ages of mafic intrusions in the age range of 319 to 310 Ma, as those reported by Montero et al. (2004) using the single-zircon stepwise evaporation $^{207}Pb/^{206}Pb$ method, have not been registered in the most recent micro-analytical studies (Bea et al. 2006; Zeck et al.

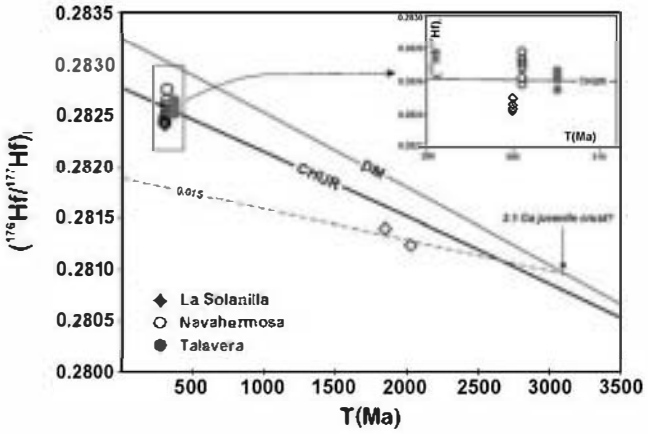

Fig. 7 Hf isotope evolution diagram for the SCS gabbros. Zircons are plotted at the crystallization age of each gabbro massif. Inherited zircons are plotted at their respective ages. Growth-curves are shown for CHUR (Blichert-Toft and Albarède 1997) and depleted mantle (DM, Griffin et al. 2000). A growth-curve with a Lu/Hf=0.015, corresponding to an averaged crustal value, is used for estimating crustal residence ages of inherited zircon protoliths. Inset shows an enlarged area of the initial $^{176}Hf/^{177}Hf$ values for the Variscan zircons

2007; present work), and have to be confirmed with further geochronological data.

Geochronological data on Variscan plutonic felsic magmatism from the Central Iberian Zone indicate that large volumes of granite were emplaced during the post-collisional stage, syn- to post-D_3 ductile deformation phase, dated at 320–312 Ma (Dias et al. 1998). Some granite intrusions are related to syn-to-late D_3 times in other sectors of the Central Iberian Zone (Dias et al. 1998; Fernández-Suárez et al. 2000a), but the SCS plutonic magmatism is mostly post-D_3, in the range of 310–295 Ma, based on recent works reporting precise U–Pb zircon geochronological results (e.g. Casquet et al. 2004; Zeck et al. 2007). Our U–Pb geochronological data reinforce the statement that Variscan gabbros in the SCS are not mafic precursors of the associated granite magmatism but mostly coeval, as largely deduced by petrological arguments (e.g. Scarrow et al. 2009; Orejana et al. 2009).

The results presented here confirm that mafic magmatism in the SCS defines a short age range of activity (307 to 300 Ma), clearly younger than the regional metamorphic peak of the sector (dated at 335–330 Ma: Escuder Viruete et al. 1998; Castiñeiras et al. 2008). All the Variscan gabbros currently dated by ion microprobe U–Pb zircon methods in central Spain yield intrusion ages within a short time span of less than 10 Ma, and they are clearly disconnected from regional heat flow Variscan events. The considerable crustal thickening attained in central Spain during syn-Variscan collision induced a later significant tectonic collapse (e.g. Escuder Viruete et al. 1998). The extensional collapse of the Variscan lithosphere and the presence of minor crustal components delaminated within the mantle during this time (e.g. Orejana et al. 2009) raise arguments for a complex flow pattern within the upper lithospheric mantle in post-Variscan stages. In this respect, recent models on gabbro generation in central Spain suggest that these mafic magmas are the result of adiabatic melting of the lithospheric mantle associated with uplift related to the post-collisional collapse of the Variscan orogen (Scarrow et al. 2009).

The age of the studied mafic magmatism is correlated with other gabbro massifs within the Central Iberian Zone: Braga (N. Portugal, around 310 Ma, Dias et al. 1998) and Vivero (N. Galicia, 293 Ma, Fernández-Suárez et al. 2000a), but also with gabbros from the Pyrenees (Querigut, 307 Ma, Roberts et al. 2000), all of them intruding during the post-collisional extension of the Variscan belt. This contrasts with data from basic massifs intruding in southern Spain, within the Ossa Morena Zone (Fig. 1), where older emplacement ages (341 to 352 Ma) and a likely transtensional post-subduction geodynamic setting have been established (Romeo et al. 2006; Pin et al. 2008).

Evidence of crustal contamination in gabbros

The scattering in Hf isotope composition of zircons and the presence of negative initial εHf values in some of the zircon populations provide evidence for the crustal contamination of gabbroic magmas, possibly in a deeper magma chamber and not at its actual emplacement level. Two processes could be envisaged to explain crustal contamination of the gabbros: a) local contamination with high-grade

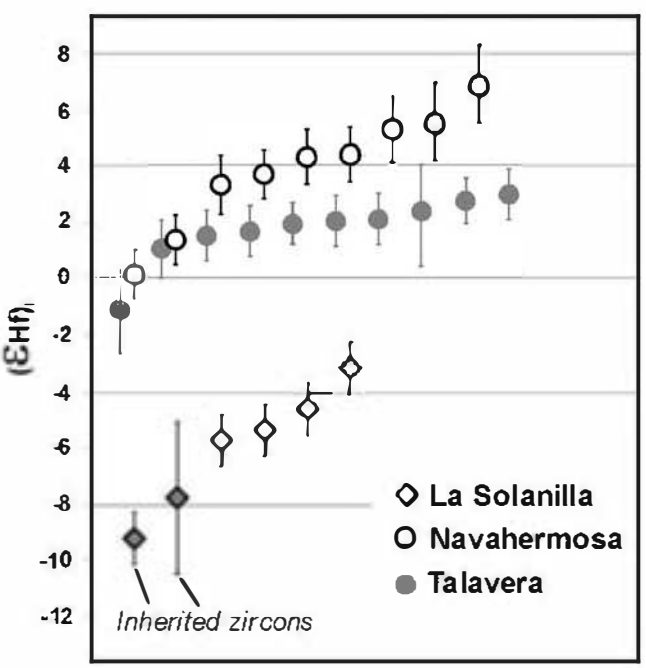

Fig. 8 Initial εHf values of individual zircon grains from each of the studied gabbro samples. The ages used to calculate the initial values are those from Table 4. εHf bars correspond to 2 σ uncertainties

metamorphic rocks (at low-to-mid crustal levels), b) magma mixing with coeval granite magmas. The lack of Hf isotope data of zircons from the different SCS lithotypes makes difficult to decide in favour of one of these models. Nevertheless, the trace element features of magmatic zircons from the SCS gabbros, showing a strong fractionation of the HREE and a low Ti concentration (<22 ppm), makes unreliable the possibility that contamination occurs with lower crustal granulites. Zircons from granulites of the SCS lower crust have high Ti contents (mostly in the range of 45 to 130 ppm) and flat HREE patterns (Órejana et al. 2011). Mixing with partial melts derived from local anatexis of high-grade metamorphic wall-rocks or, alternatively, mixing and hybridization with Variscan granite magmas (which in some outcrops are intermingled with the studied gabbros, e.g. Navahermosa), are more plausible contamination processes. In either case, mixing with granitic melts, from local surrounding rocks or by interaction with allochthonous ascending melts, is the main contaminant source for crustal zircons found in the SCS gabbros.

According to Hf-isotope composition, zircons show a variable but increasing degree of granite magma contamination from Talavera and Navahermosa to La Solanilla gabbros. The crustal contamination of the Talavera gabbro is minor. In this sample, excepting one zircon showing clear negative initial εHf values (−1.1; T46-19.1 spot, Table 4) the rest of values group around +2±0.9, with a variation close to analytical uncertainties (Fig. 8). Hf isotope data in zircons from Navahermosa gabbro mostly group in the range of +3.3 to +6.9, with a variation that clearly exceeds the analytical uncertainties. Moreover, this range is three epsilon units higher than those from Talavera gabbro. This difference is supported by the whole-rock initial εNd values (+1.55 for Navahermosa versus −1.6 for Talavera gabbros; Órejana et al. 2009). Combined Hf and Nd isotope signatures therefore suggest different mantle sources for the SCS gabbroic magmas, with Navahermosa derived from a more depleted mantle source than the Talavera gabbro. Nevertheless, the larger variation in εHf values of the Navahermosa gabbro (Fig. 8), suggest higher crustal contamination rates in this massif.

Magmatic zircons from La Solanilla gabbro show the most evolved Hf-isotope composition encountered in the SCS gabbros (Table 4; Fig. 8). No vestiges of mantle-derived zircons are found in this sample. Thus, these Variscan zircon grains should be considered as antecrysts derived from likely coeval felsic magmas. They represent an isotopically distinct magma batch incorporated into the basic magmatic system. Accordingly, the concordia age obtained for this sample must be considered as a maximum estimate of its emplacement age.

The presence of zircon grains with crustal isotopic signatures in the studied gabbroic samples is in agreement with models of significant assimilation of crustal components by the SCS gabbroic magmas (Molina et al. 2009) and with the previously described conspicuous presence of accessory phases of crustal origin (Bea et al. 1999).

Significance of Proterozoic inheritances

Two zircon crystals from La Solanilla massif gave slightly discordant (discordancy <10%) Paleoproterozoic ages (1,800 to 2,100 Ma). The preservation of inherited zircons in ultramafic-mafic rocks is not unusual but is rarely described in Variscan to post-Variscan gabbros (Gebauer et al. 1992; Peressini et al. 2007; Renna and Tribuzio 2009). To our knowledge this is the first report of zircon inheritances in Variscan Mg-rich gabbros from central Spain; only Montero et al. (2004b) reported Palaeoproterozoic ages for xenocrystic zircons, but in a highly hybridized dioritic rock. Zircon inheritances in mantle-derived rocks can be explained by: a) contamination with crustal material during transport or emplacement (e.g. Schwartz et al. 2005; Whattam et al. 2006), b) delaminated lower crustal slices at mantle depths (Pilot et al. 1998; Rubatto et al. 1998), or c) incorporation of xenocrysts from metasomatized subcontinental mantle (e.g. Peltonen et al. 2003). The markedly evolved Hf signature of the pre-Variscan zircons of La Solanilla gabbros (εHf from −8.1 to −10.7; Table 4), suggest that these zircons have been incorporated into the mafic magma during its transport within the crust, and a mantle origin is therefore unlikely.

The low Ti measured in pre-Variscan zircons from gabbros (from 10 to 14 ppm, Table 2) is within the range of Ti concentrations of zircons from granitoids from central Spain (3.6 to 24 ppm, unpublished data). The presence of Proterozoic inherited zircons in granites from the SCS (Zeck et al. 2007) and other felsic intrusions from the Central Iberian Zone (e.g. Solá et al. 2009) reinforces the possibility of incorporation of both magmatic and inherited crystals during the mixing with granitic melts.

Inherited Paleoproterozoic zircon ages have also been recorded in Neoproterozoic metasediments from the Central Iberian Zone (e.g. Fernández-Suárez et al. 2000b; Montero et al. 2007), although representing a minor age population. Nd model ages (T_{DM} values) calculated for granitic and metasedimentary rocks from central Spain yield values of 1.4–1.6 and 1.6–2.0 Ga, respectively (data from Table 3 of Villaseca et al. 1998). Nevertheless, an important juvenile addition during the Early Proterozoic is not in agreement with the Hf isotope composition of the inherited zircons from the La Solanilla gabbro.

By combining the $^{176}Hf/^{177}Hf$ from inherited zircons with an averaged crustal Lu/Hf ratio of 0.015 (Griffin et al.

2002) is possible to estimate Lu-Hf model ages and the crustal residence age of their protoliths (e.g. Andersen et al. 2002). Obtained T_{DM2} model ages of 3.0 to 3.2 Ga (Table 4) are much older than those estimated by whole-rock Nd isotopes. To our knowledge, this is the first recognition, in the Iberian Variscan Belt, of recycled Archean material within the source of granitic protoliths incorporated in coevally hybridized gabbroic magmas. A juvenile addition during the Early Archean is in accordance with some of the major times of continental growth (e.g. Condie and Aster 2010), and with detrital zircon results (e.g. Iizuka et al. 2010).

Nature of the Variscan lithospheric mantle

The zircon Lu–Hf isotope data is a sensitive tracer of the processes that affected the gabbroic magmas (e.g. Peytcheva et al. 2008). The large scattering in initial εHf of zircons evidences significant contamination processes in the gabbroic magmas. Nevertheless, positive initial εHf values are representative of the mantle-derived component in the studied Variscan gabbros. Our data reveal that the most positive εHf_i values are between +3.6 to +6.9 in the Navahermosa gabbro, whereas they range from +1.5 to +2.9 in the Talavera gabbro. Thus, values from +1.5 to +6.9 might represent the composition of the Variscan subcontinental mantle beneath this sector of central Spain. This range is clearly below that of depleted mantle (+15 to +17) or recent Atlantic MORB (+8 to +21; Chauvel and Blichert-Toft 2001). Heterogeneous but enriched mantle components might be involved in the genesis of these gabbroic magmas, as was also stated by whole-rock studies, including Sr–Nd–Pb isotopes (e.g. Scarrow et al. 2009; Orejana et al. 2009).

Most of the Carboniferous-Permian mafic magmatism in the Central Iberian Zone and the Pyrenees also show evolved Sr and Nd isotope signatures, and its primitive chemical character suggests that extensive crustal contamination during transport is unlikely (e.g. Dias et al. 2002). This also precludes an origin from a depleted mantle source.

Part of the Variscan mafic magmatism of similar age (300–316 Ma) in Europe is characterized by K-rich rocks showing strong enrichment in LILE and REE (and evolved Sr and Nd isotope ratios), indicating an affinity to K-rich calc-alkaline magmas (e.g. Turpin et al. 1998; Hegner et al. 1998). Most of them have been interpreted as derived from a crust-contaminated mantle source, and likely resulted from post-collisional melting of subducted or delaminated lithosphere (e.g. Neubauer et al. 2003). An enriched lithospheric mantle is also envisaged for central Spain during most of the Upper Carboniferous to Lower Permian period (Villaseca et al. 2004). It seems that in the Central and Western European Variscides an enriched upper mantle was available until around 285 Ma. At that time transitional, tholeiitic and alkaline basic magmas appear in central and south-central Europe, suggesting an apparent replacement of lithospheric mantle by more depleted (asthenospheric) sources (e.g. Monjoie et al. 2007; Renna et al. 2007). In central Spain the intrusion of alkaline lamprophyres around 260 Ma represents the incoming of depleted mantle compositions (Orejana et al. 2008).

Acknowledgments We acknowledge Alfredo Fernández Larios and José González del Tánago for their assistance with the electron microprobe analyses in the CAI of Microscopía Electrónica (Complutense University of Madrid). We are also grateful to Norman Pearson and Rosanna Murphy for their help while performing Hf isotope analyses. We also thank Rosanna Murphy for improving the English. Editorial handling by Johann G. Raith and suggestions made by two anonymous reviewers have greatly increased the quality of the final version of the manuscript. This work is included in the objectives of, and supported by, the CGL2008-05952 project of the Ministerio de Ciencia y Tecnología of Spain and the GR58/08-910492-UCM project.

References

Andersen T, Griffin WL, Pearson NJ (2002) Crustal evolution in the SW part of the Baltic Shield: the Hf isotope evidence. J Petrol 43:1725–1747

Austrheim H, Putnis CV, Engivk AK, Putnis A (2008) Zircon coronas around Fe–Ti oxides: a physical reference frame for metamorphic and metasomatic reactions. Contrib Mineral Petrol 156:517–527

Bea F, Montero P, Molina JF (1999) Mafic precursors, peraluminous granitoids, and late lamprophyres in the Avila batholith; a model for the generation of Variscan batholiths in Iberia. J Geol 107:399–419

Bea F, Montero P, Zinger T (2003) The nature, origin, and thermal influence of the granite source layer of Central Iberia. J Geol 111:579–595

Bea F, Montero PG, González-Lodeiro F, Talavera C, Molina JF, Scarrow JH, Whitehouse MJ, Zinger T (2006) Zircon thermometry and U–Pb ion-microprobe dating of the gabbros and associated migmatites of the Variscan Toledo anatectic complex, central Iberia. J Geol Soc Lond 163:847–855

Belousova EA, Griffin WL, O'Reilly SY (2006) Zircon crystal morphology, trace-element signatures and Hf-isotope composition as a tool for petrogenetic modelling: examples from eastern Australian granitoids. J Petrol 47:329–353

Black LP, Kamo SL, Allen CM, Aleinikoff JN, Davis DW, Korsch RJ, Foudoulis C (2003) TEMORA 1: a new zircon standard for Phanerozoic U–Pb geochronology. Chem Geol 200:155–170

Black LP, Kamo SL, Allen CM, Davis DW, Aleinikoff JN, Valley JW, Mundil R, Campbell IH, Korsch RJ, Williams IS, Foudoulis C (2004) Improved $^{206}Pb/^{238}U$ microprobe geochronology by the monitoring of a trace-element-related matrix effect; SHRIMP, ID-TIMS, ELA-ICP-MS and oxygen isotope documentation for a series of zircon standards. Chem Geol 205:115–140

Blichert-Toft J, Albarède F (1997) The Lu–Hf geochemistry of chondrites and the evolution of the mantle-crust system. Earth Planet Sci Lett 148:243–258

Bouvier A, Vervoot JD, Patchett PJ (2008) The Lu–Hf and Sm–Nd isotopic composition of CHUR: constraints from unequilibrated chondrites and implications for the bulk composition of terrestrial planets. Earth Planet Sci Lett 273:48–57

Casillas R, Vialette Y, Peinado M, Duthou JL, Pin C (1991) Âges et caractéristiques isotopiques (Sr, Nd) des granitoïdes de la Sierra de Guadarrama occidentale (Espagne). Abstract Séance Spécialisée Soc Géol France, Mémoire Jean Lameyre.

Casquet C, Montero P, Galindo C, Bea F, Lozano R (2004) Geocronología $^{207}Pb/^{206}Pb$ en cristal único de circón y Rb–Sr del plutón de La Cabrera (Sierra del Guadarrama). Geogaceta 35:71–74

Castiñeiras P, Villaseca C, Barbero L, Martín Romera C (2008) SHRIMP U–Pb zircon dating of anatexis in high-grade migmatite complexes of Central Spain: implications in the Hercynian evolution of central Iberia. Int J Earth Sci 97:35–50

Castro A, Patiño Douce AE, Corretgé LG, de la Rosa J, El-Biad M, El-Hmidi H (1999) Origin of peraluminous granites and granodiorites, Iberian massif, Spain: an experimental test of granite petrogenesis. Contrib Mineral Petrol 135:255–276

Chauvel C, Blichert-Toft J (2001) A hafnium isotope and trace element perspective on melting of the depleted mantle. Earth Planet Sci Lett 190:137–151

Condie KC, Aster RC (2010) Episodic zircon age spectra of orogenic granitoids: the supercontinent connection and continental growth. Precambrian Res 180:227–236

Dias G, Leterrier J, Mendes A, Simoes PP, Bertrand JM (1998) U–Pb zircon and monazite geochronology of syn- to post-tectonic Hercynian granitoids from the Central Iberian Zone (Northern Portugal). Lithos 45:349–369

Dias G, Simoes PP, Ferreira N, Leterrier J (2002) Mantle and crustal sources in the genesis of late-Hercynian granitoids (NW Portugal): geochemical and Sr–Nd isotopic constraints. Gondwana Res 5:287–305

Escuder Viruete J, Hernáiz PP, Valverde-Vaquero P, Rodríguez R, Dunning G (1998) Variscan syncollisional extension in the Iberian Massif: structural, metamorphic and geochronological evidence from the Somosierra sector of the Sierra de Guadarrama (Central Iberian Zone, Spain). Tectonophysics 290:87–109

Fernández-Suárez J, Dunning GR, Jenner GA, Gutiérrez-Alonso G (2000a) Variscan collisional magmatism and deformation in NW Iberia: constraints from U–Pb geochronolgy of granitoids. J Geol Soc Lond 157:565–576

Fernández-Suárez J, Gutiérrez-Alonso G, Jenner GA, Tubrett MN (2000b) New ideas on the Proterozoic-early Palaeozoic evolution of NW Iberia: insights from U–Pb detrital zircon ages. Precambrian Res 102:185–206

Ferry JM, Watson EB (2007) New thermodynamic models and revised calibration for the Ti-in-zircon and Zr-in-rutile thermometers. Contrib Mineral Petrol 154:429–437

Franco MP (1980) Estudio petrológico de las formaciones metamórficas y plutónicas al norte de la depresión del Corneja-Amblés (Sierra de Ávila). Ph. D. Thesis, Universidad de Salamanca, pp 273

Franco MP, García de Figuerola LC (1986) Las rocas básicas y ultrabásicas en el extremo occidental de la Sierra de Ávila. Studia Geol Salmant 23:193–219

Franco MP, Sánchez García T (1987) Características petrológicas del área de El Mirón. In: Bea F, Camicero A, Gonzalo JC, López Plaza M, Rodríguez Alonso MD (eds) Geología de los granitoides y rocas asociadas del Macizo Hespérico. Rueda, Madrid, pp 293–313

Fu B, Page FZ, Cavosie AJ, Fournelle J, Kita NT, Lackey JS, Wilde SA, Valley JW (2008) Ti-in-zircon thermometry: applications and limitations. Contrib Mineral Petrol 156:197–215

Gebauer D, Schmidt R, von Quadt A, Ulmer P (1992) Oligocene, Permian and Panafrican zircon ages from rocks of the Balmuccia Peridotite and of the Lower Layered Group in the Ivrea Zone. Schweiz Miner Petrogr Mitt 72:113–122

Griffin WL, Pearson NJ, Belousova E, Jackson SE, van Achterbergh E, O'Reilly SY, Shee SR (2000) The Hf isotope composition of cratonic mantle: LAM-MC-ICPMS analysis of zircon megacrysts in kimberlite. Geochim Cosmochim Acta 64:133–147

Griffin WL, Wang X, Jackson SE, Pearson NJ, O'Reilly SY, Xu X, Zhou X (2002) Zircon chemistry and magma mixing, SE China: in situ analysis of Hf isotopes, Tonglu and Pingtan igneous complexes. Lithos 61:237–269

Griffin WL, Belousova E, Shee SR, Pearson NJ, O'Reilly SY (2004) Archean crustal evolution in the northern Yilgarn Craton: U–Pb and Hf isotope evidence from detrital zircons. Precambrian Res 131:231–282

Grimes CB, John BE, Kelemen PB, Mazdab FK, Wooden JL, Cheadle MJ, Hanghoj K, Schwartz JJ (2007) Trace element chemistry of zircons from oceanic crust: a method for distinguishing detrital zircon provenance. Geology 35:643–646

Grimes CB, John BE, Cheadle MJ, Mazdab FK, Wooden JL, Swapp S, Schwartz JJ (2009) On the occurrence, trace element geochemistry, and crystallization history of zircon from in situ ocean lithosphere. Contrib Mineral Petrol 158:757–783

Hegner E, Kölbl-Ebert M, Loeschke J (1998) Post-collisional Variscan lamprophyres (Black Forest, Germany): $^{40}Ar/^{39}Ar$ phlogopite dating, Nd, Pb, Sr isotope, and trace element characteristics. Lithos 45:395–411

Hoskin PWO, Schaltegger U (2003) The composition of zircon in igneous and metamorphic petrogenesis. In: Hanchar JM, Hoskin POW (eds) Zircon. Rev Mineral Geochem 53:27–62

Iizuka T, Komiya T, Rino S, Maruyama S, Hirata T (2010) Detrital zircon evidence for Hf isotopic evolution of granitoid crust and continental growth. Geochim Cosmochim Acta 74:2450–2472

Jarosewich EJ, Boatner LA (1991) Rare-earth element reference samples for electron microprobe analysis. Geostand Newsl 15:397–399

Liew TC, Finger F, Höck V (1989) The Moldanubian granitoid plutons of Austria: chemical and isotopic studies bearing on their environmental setting. Chem Geol 76:41–55

Ludwig KR (2001) SQUID 1.02, a user's manual. Berkeley Geochronological Center Special Public 2:1–17

Ludwig KR (2003) ISOPLOT/Ex, version 3, a geochronological toolkit for microsoft excel. Berkeley Geochronological Center Special Public 4:1–71

Martín Parra LM, Martínez Salanova J, Marqués Calvo LA, Contreras E, Iglesias A, Martín Herrero D (1995) Memoria Hoja 602 (Navamorcuende) MAGNA 1:50.000. IGME, Madrid, p 84

Miller JS, Matzel JEP, Miller CF, Burgess SD, Miller RB (2007) Zircon growth and recycling during the assembly of large, composite arc plutons. J Volcan Geotherm Res 167:282–299

Molina JF, Scarrow JH, Montero P, Bea F (2009) High-Ti amphibole as a petrogenetic indicator of magma chemistry: evidence for mildly alkalic-hybrid melts during evolution of Variscan basic-ultrabasic magmatism of Central Iberia. Contrib Mineral Petrol 158:69–98

Monjoie P, Bussy F, Schaltegger U, Mulch A, Lapierre H, Pfeifer HR (2007) Contrasting magma types and timing of intrusion in the Permian layered mafic complex of Mont Collon (Western Alps, Valais, Switzerland): evidence from U–Pb zircon and $^{40}Ar/^{39}Ar$ amphibole dating. Swiss J Geosci 100:125–135

Montero P, Bea F, Zinger T (2004) Edad $^{207}Pb/^{206}Pb$ en cristal único de circón de las rocas máficas y ultramáficas del sector de Gredos, batolito de Ávila (sistema central español). Rev Soc Geol Esp 17:157–167

Montero P, Bea F, González-Lodeiro F, Talavera C, Whitehouse MJ (2007) Zircon ages of the metavolcanic rocks and metagranites of the Ollo de Sapo Domain in central Spain: implications for the Neoproterozoic to Early Palaeozoic evolution of Iberia. Geol Mag 144:963–976

Moreno-Ventas I, Rogers G, Castro A (1995) The role of hybridization in the genesis of Hercynian granitoids in the Gredos Massif, Spain: inferences from Sr–Nd isotopes. Contrib Mineral Petrol 120:137–149

Morisset C-E, Scoates S (2008) Origin of zircons rims around ilmenite in mafic plutonic rocks of Proterozoic anorhtosite suites. Can Mineral 46:289–304

Naslund HR (1987) Lamellae of baddeleyite and Fe–Cr spinel in ilmenite from the Basistoppen Sill, East Greenland. Can Mineral 25:91–96

Neubauer F, Dallmeyer RD, Fritz H (2003) Chronological constraints of late- and post-orogenic emplacement of lamprophyric dykes in the southeastern Bohemian Massif, Austria. Schweiz Miner Petrogr Mitt 83:317–330

Orejana D, Villaseca C, Billström K, Paterson BA (2008) Petrogenesis of Permian alkaline lamprophyres and diabases from the Spanish Central System and their geodynamic context within western Europe. Contrib Mineral Petrol 156:477–500

Orejana D, Villaseca C, Pérez-Soba C, López-García JA, Billstrom K (2009) The Variscan gabros from the Spanish Central System: a case for crustal recycling in the subcontinental lithospheric mantle? Lithos 110:262–276

Orejana D, Villaseca C, Armstrong RA, Jeffries T (2011) Geochronology and trace element chemistry of zircon and garnet from granulite xenoliths: constraints on the tectonothermal evolution of the lower crust under central Spain. Lithos. doi:10.1016/j.lithos.2010.10.011

Peltonen P, Mänttäri I, Huhma H, Kontinen A (2003) Archean zircons from the mantle: the Jormua ophiolite revisited. Geology 31:645–648

Pereira MD, Ronkin Y, Bea F (1992) Dataciones Rb/Sr en el complejo anatéctico de la Peña Negra (Batolito de Ávila, España central): evidencias de magmatismo pre-hercínico. Rev Soc Geol Esp 5:129–134

Peressini G, Quick JE, Sinigoi S, Hofmann AW, Fanning M (2007) Duration of a large mafic intrusion and heat transfer in the lower crust: a SHRIMP U–Pb zircon study in the Ivrea-Verbano Zone (Western Alps). J Petrol 48:1185–1218

Peytcheva I, von Quadt A, Georgiev N, Ivanov Zh, Heinrich CA, Frank M (2008) Combining trace-element compositions, U–Pb geochronology and Hf isotopes in zircons to unravel complex calc-alkaline magma chambers in the Upper Cretaceous Sredno-gorie zone (Bulgaria). Lithos 104:405–427

Pilot J, Werner C-D, Haubrich F, Baumann N (1998) Palaeozoic and Proterozoic zircons from the Mid-Atlantic Ridge. Nature 393:676–679

Pin C, Fonseca PE, Paquette JL, Castro P, Matte Ph (2008) The ca. 350 Ma Beja igneous complex: a record of transcurrent slab break-off in the Southern Iberian Variscan Belt? Tectonophysics 461:356–377

Pinarelli L, Rottura A (1995) Sr and Nd isotopic study and Rb–Sr geochronology of the Béjar granites, Iberian Massif, Spain. Eur J Mineral 7:577–589

Renna MR, Tribuzio R (2009) Petrology, geochemistry and U–Pb zircon geochronology of lower crust pyroxenites from northern Appennine (Italy): insights into the post-collisional Variscan evolution. Contrib Mineral Petrol 157:813–835

Renna MR, Tribuzio R, Tiepolo M (2007) Origin and timing of the post-Variscan gabbro-granite complex of Porto (Western Corsica). Contrib Mineral Petrol 154:493–517

Roberts MP, Pin C, Clemens JD, Paquette JL (2000) Petrogenesis of mafic to felsic plutonic rock association: the calc-alkaline Quérigut Complex, French Pyrenees. J Petrol 41:809–844

Romeo I, Lunar R, Capote R, Quesada C, Dunning GR, Piña R, Ortega L (2006) U–Pb age constraints on Variscan magmatism and Ni-Cu-PGE metallogeny in the Ossa-Morena Zone (SW Iberia) J Geol Soc London 163:837–846

Rubatto D, Hermann J (2007) Zircon behaviour in deeply subducted rocks. Elements 3:31–35

Rubatto D, Gebauer D, Fanning CM (1998) Jurassic formation and Eocene subduction of the Zermatt-Saas-Fee ophiolites: implications for the geodynamic evolution of the central and western Alps. Contrib Mineral Petrol 132:269–287

Scarrow J, Molina JF, Bea F, Montero P (2009) Within-plate calc-alkaline rocks: insights from alkaline mafic magma-peraluminous crustal melt hybrid appinites of the Central Iberian Variscan continental collision. Lithos 110:50–64

Scherer EE, Münker C, Mezger K (2001) Calibration of the lutetium-hafnium clock. Science 293:683–687

Schwartz JJ, John BE, Cheadle MJ, Grimes C, Miranda EA, Wooden JL, Dick HJB (2005) Inherited zircon and the magmatic construction of oceanic crust. Geochim Cosmochim Acta 69 (10):A294

Solá AR, Williams IS, Neiva AMR, Ribeiro ML (2009) U–Th–Pb SHRIMP ages and oxygen isotope composition of zircon from two contrasting late Variscan granitoids, Nisa-Alburquerque batholith, SW Iberian Massif: petrologic and regional implications. Lithos 111:156–167

Sun SS, McDonough WF (1989) Chemical and isotopic systematic of oceanic basalts; implications for mantle composition and processes. Geol Soc Lond Spec Publ 42:313–345

Tera F, Wasseburg GJ (1972) U–Th–Pb systematics in three Apollo 14 basalts and the problem of initial Pb in lunar rocks. Earth Planet Sci Lett 14:281–304

Turpin L, Velde D, Pinte G (1988) Geochemical comparison between minettes and kersantites from the Western European Hercynian orogen: trace element and Pb–Sr–Nd isotope constraints on their origin. Earth Planet Sci Lett 87:73–86

Ugidos JM, Recio C (1993) Origin of cordierite-bearing granites by assimilation in the Central Iberian Massif (CIM), Spain. Chem Geol 103:27–43

Villaseca C, Herreros V (2000) A sustained felsic magmatic system: the Hercynian granitic batholith of the Spanish Central System. Trans R Soc Edinb Earth Sci 91:207–219

Villaseca C, Barbero L, Rogers G (1998) Crustal origin of Hercynian peraluminous granitic batholiths of Central Spain: petrological, geochemical and isotopic (Sr, Nd) constraints. Lithos 43:55–79

Villaseca C, Downes H, Pin C, Barbero L (1999) Nature and composition of the lower continental crust in central Spain and the granulite-granite linkage: inferences from granulitic xenoliths. J Petrol 40:1465–1496

Villaseca C, Orejana D, Pin C, López-García JA, Andonaegui P (2004) Le magmatisme basique hercynien et post-hercynien du Systéme central espagnol: essai de caractérisation des sources mantelliques. C R Geosci 336:877–888

Villaseca C, Orejana D, Paterson BA, Billström K, Pérez-Soba C (2007) Metaluminous pyroxene-bearing granulite xenoliths from the lower continental crust in central Spain: their role in the genesis of Hercynian I-type granites. Eur J Mineral 19:463–477

Watson EB, Wark DA, Thomas JB (2006) Crystallization thermometers for zircon and rutile. Contrib Mineral Petrol 151:413–433

Wetherill GW (1956) Discordant uranium-lead ages. Trans Am Geophys Union 37:320–326

Whattam SA, Malpas J, Smith IEM, Ali JR (2006) Link between SSZ ophiolite formation, emplacement and arc inception, Northland, New Zealand: U–Pb SHRIMP constraints; Cenozoic SW Pacific tectonic implications. Earth Planet Sci Lett 250:606–632

Williams IS (1998) U–Th–Pb geochronology by ion microprobe. In: McKibben MA, Shanks WCP, Ridley WI (eds) Applications of microanalytical techniques to understanding mineralizing processes. Rev Econ Geol 7:1–35

Woodhead JD, Hergt JM (2005) A preliminary appraisal of seven natural zircon reference materials for in situ Hf isotope determinations. Geostand Geoanal Res 29:183–195

Zeck HP, Wingate MTD, Pooley G (2007) Ion microprobe U–Pb zircon geochronology of a late tectonic granitic-gabbroic rock complex within the Hercynian Iberian belt. Geol Mag 144:157–177